Evaluation of a (131°,90°) Physics Optics for LEP

John M. Jowett

24 November 1998

Abstract

A new optics with phase advances $\mu_x = 131\,°$ and $\mu_y = 90\,°$ in the arc cells has been proposed for LEP. This note summarises the main results from the optics evaluation procedure that is now routinely applied to new LEP optics. This includes the study of the orbits, optics and dynamic apertures of an ensemble of imperfect machines with corrections similar to those applied in operation. It provides predictions of performance and results of measurements that can be done when the optics is commissioned.

The results show that the dynamic aperture of this optics is much smaller than necessary for high-energy operation of LEP. A modification of the sextupole configuration to reduce the detuning with amplitude does not help.

Introduction

To evaluate the potential performance of a new optics for LEP, it is necessary to perform calculations of orbits, optics, beam parameters and dynamic apertures on an ensemble of imperfect machines. Over the last few years, a standard procedure has evolved for this purpose. It has been applied to a "squeezed" (131°,90°) physics optics at 94 GeV, prepared by A. Verdier in summer 1998. This optics uses three families of SF sextupoles and two of SD.

The procedure followed is outlined in the note [1] which gave the corresponding results for the (102°,90°) tested in late 1997 at a lower energy. There is some additional discussion in [2]. To make it easy to compare (and for me to write), the results are presented in the same format although some sections have been cut out. Many further results can be extracted from the publicly available database generated by the evaluation procedure.

Full details of the configuration and the calculations can be found using the following information:

k348physA3n3 by AV, 131/90 for 1998 94 GeV

```
MAD working directory was:
/afs/cern.ch/eng/lep/imperf/lep98/k368physA3n3
Current directory: J:\lep98\imperf\k368physA3n3
```

2 Remarks on the results

It was possible to find and correct the average closed orbit for all 30 machines.   All machines remained stable for both particle types when the solenoids and their computed coupling compensation with tilted quadrupoles were switched on *and* when radiation was switched on.

In the following, the means, standard deviations and other statistical quantities refer to the distribution of quantities over the ensemble of 30 machines. The estimator for standard deviation quoted is always unbiased although it could be argued that a maximum-likelihood estimate (4% smaller here) would be justified for some physical quantities. In this note, I also make the point that the *harmonic mean* has greater physical relevance for the vertical emittance than the usual mean.

Because of the strong radiation effects, the orbit and optics are different for the two beams. Therefore many quantities are given for both electrons and positrons. Some quantities, such as the tune splits or centre-of-mass energies, have to be derived by combining properties of the two beams.

3 RF configuration

It was assumed, rather idealistically, that each superconducting RF unit provided a peak voltage of 42 MV and each copper one 2.2 MV and that all units were properly phased. The 1998 configuration resulted in the distribution of RF voltage by octant of LEP shown in Figure 1. The total voltage is more than the minimum necessary for the beam energy.

Figure 1
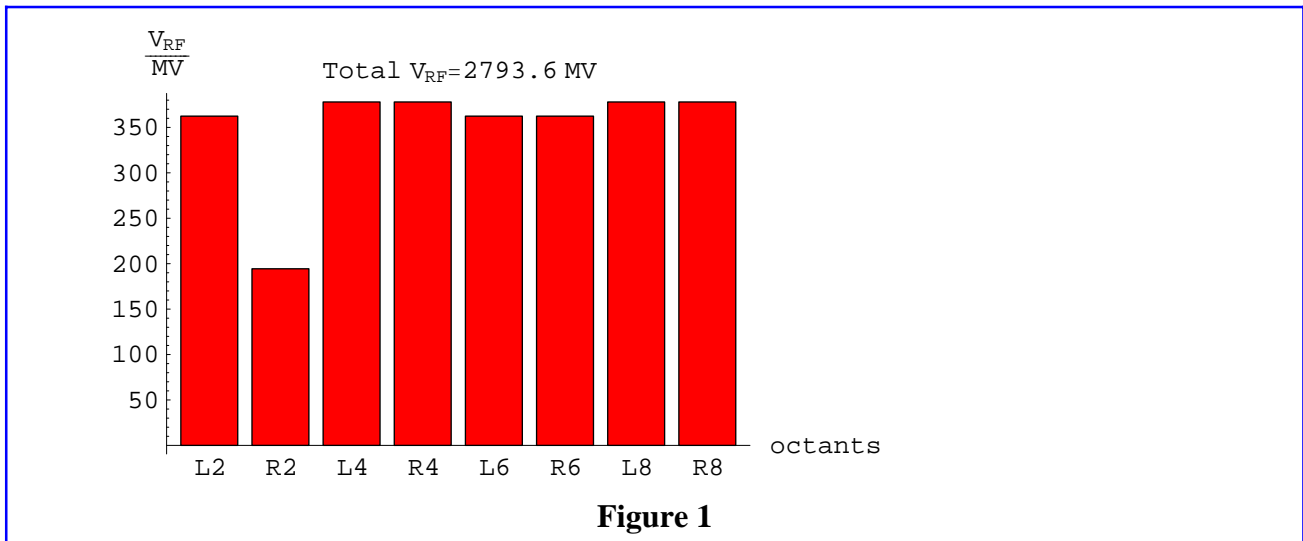
- Graphics -

4 Orbits and optics

The imperfections of each machine in the ensemble give rise to different closed orbits after correction. Furthermore, in a given machine, the positrons and electrons, despite seeing the same imperfections, move in opposite directions around the ring. Since the terms in their equations of motion describing synchrotron radiation are not time-reversal invariant, they have very different closed orbits (separated horizontally by several mm in some places). The optical functions codify the behaviour of small displacements from these closed orbits and these, too, will differ from machine to machine and from one beam to the other. This section summarises the statistical information on orbits, optical functions and derived quantities such as the separations at the interaction points (IPs).

4.1 Global optical parameters

Table 1 lists the statistics for a number of global quantities related to the optics.   Some of these are derived from the traditional Courant-Snyder (labelled "CS" in the table) calculations and may not take proper account of the radiation and RF effects but still have some indicative value. The tunes quoted are the correct tunes on the 6-dimensional closed orbit.

Quantity	Symbol	Mean	σ_{est}	Units
Momentum compaction for e^+	$\alpha_c{}^+$	0.0001076	5.6×10^{-8}	
Momentum compaction for e^-	$\alpha_c{}^-$	0.0001076	5.59×10^{-8}	
Max. horizontal CS β-function for e^+	$\beta_x^{\max+}$	516.6	103.	m
Max. horizontal CS β-function for e^-	$\beta_x^{\max-}$	493.9	115.	m
Max. vertical CS β-function for e^+	$\beta_y^{\max+}$	477.6	14.7	m
Max. vertical CS β-function for e^-	$\beta_y^{\max-}$	411.4	7.62	m
Horizontal tune for e^+	$Q_1{}^+$	0.2801	0.0000711	
Horizontal tune for e^-	$Q_1{}^-$	0.2918	0.00954	
Vertical tune for e^+	$Q_2{}^+$	0.1906	0.0000419	
Vertical tune for e^-	$Q_2{}^-$	0.217	0.00293	
Synchrotron tune for e^+	$Q_3{}^+$	0.09569	0.0000433	
Synchrotron tune for e^-	$Q_3{}^-$	0.0957	0.0000308	
Horizontal tune split	$\triangle Q_1{}^\pm$	-0.01173	0.00953	
Vertical tune split	$\triangle Q_2{}^\pm$	-0.02642	0.00293	
Horizontal CS chromaticity for e^+	$Q_x{}'^+$	0.2668	1.99	
Horizontal CS chromaticity for e^-	$Q_x{}'^-$	0.5856	1.57	
Vertical CS chromaticity for e^+	$Q_y{}'^+$	0.3289	0.459	
Vertical CS chromaticity for e^-	$Q_y{}'^-$	0.8314	0.415	
Horizontal chromaticity split	$\triangle Q_x{}'^\pm$	-0.3188	1.32	
Vertical chromaticity split	$\triangle Q_y{}'^\pm$	-0.5024	0.402	

Table 1

Since the tune correction for each machine was done on the positrons, the tunes of the positron beams have a very small spread while the electrons are left with a certain spread. The vertical tune-split is relatively small, thanks to the fairly symmetric RF voltage distribution.

4.2 Global orbits

Table 2 gives some global orbit parameters, where notations like $\overline{x^2}$ denote averages around the ring. The *average* $e^+ e^-$ orbit was corrected to 0.6 and 0.4 mm RMS in the horizontal and vertical planes. The larger RMS values for individual beams in the horizontal plane reflect the energy-sawtoothing.

Quantity	Symbol	Mean	σ_{est}	Units
RMS horizontal orbit for e^+	$\sqrt{\overline{x^2}}{}^+$	1.435	0.0657	mm
RMS horizontal orbit for e^-	$\sqrt{\overline{x^2}}{}^-$	1.446	0.0733	mm
Max. horizontal orbit for e^+	$x_{\max}{}^+$	7.596	0.958	mm
Max. horizontal orbit for e^-	$x_{\max}{}^-$	7.668	0.988	mm
RMS vertical orbit for e^+	$\sqrt{\overline{y^2}}{}^+$	0.3763	0.0482	mm
RMS vertical orbit for e^-	$\sqrt{\overline{y^2}}{}^-$	0.3655	0.0319	mm
Max. vertical orbit for e^+	$y_{\max}{}^+$	1.621	0.195	mm
Max. vertical orbit for e^-	$y_{\max}{}^-$	1.593	0.18	mm

Table 2

4.3 Orbits and separations at the interaction points

More detailed information about the orbits at the interaction points is given in Table 3.

Quantity		Mean	σ(est)	Units
Horizontal orbit for e$^+$[IP2]	x(IP2)$^+$	-0.02007	0.209	mm
Horizontal orbit for e$^-$[IP2]	x(IP2)$^-$	-0.02985	0.202	mm
Horizontal orbit for e$^+$[IP4]	x(IP4)$^+$	0.05885	0.218	mm
Horizontal orbit for e$^-$[IP4]	x(IP4)$^-$	0.05338	0.217	mm
Horizontal orbit for e$^+$[IP6]	x(IP6)$^+$	0.003214	0.19	mm
Horizontal orbit for e$^-$[IP6]	x(IP6)$^-$	-0.0106	0.193	mm
Horizontal orbit for e$^+$[IP8]	x(IP8)$^+$	0.04006	0.209	mm
Horizontal orbit for e$^-$[IP8]	x(IP8)$^-$	0.04849	0.22	mm
Horizontal separation [IP2]	$\triangle$x$^\pm$[IP2]	0.009785	0.0426	mm
Horizontal separation [IP4]	$\triangle$x$^\pm$[IP4]	0.005476	0.0519	mm
Horizontal separation [IP6]	$\triangle$x$^\pm$[IP6]	0.01381	0.0555	mm
Horizontal separation [IP8]	$\triangle$x$^\pm$[IP8]	-0.008438	0.0594	mm
Vertical orbit for e$^+$[IP2]	y(IP2)$^+$	0.01852	0.134	mm
Vertical orbit for e$^-$[IP2]	y(IP2)$^-$	0.01824	0.134	mm
Vertical orbit for e$^+$[IP4]	y(IP4)$^+$	0.01158	0.11	mm
Vertical orbit for e$^-$[IP4]	y(IP4)$^-$	0.01208	0.11	mm
Vertical orbit for e$^+$[IP6]	y(IP6)$^+$	-0.03372	0.128	mm
Vertical orbit for e$^-$[IP6]	y(IP6)$^-$	-0.03344	0.128	mm
Vertical orbit for e$^+$[IP8]	y(IP8)$^+$	0.02026	0.119	mm
Vertical orbit for e$^-$[IP8]	y(IP8)$^-$	0.02013	0.119	mm
Vertical separation [IP2]	$\triangle$y$^\pm$[IP2]	0.0002802	0.00261	mm
Vertical separation [IP4]	$\triangle$y$^\pm$[IP4]	-0.0004984	0.00363	mm
Vertical separation [IP6]	$\triangle$y$^\pm$[IP6]	-0.0002796	0.00314	mm
Vertical separation [IP8]	$\triangle$y$^\pm$[IP8]	0.0001282	0.00251	mm

Table 3

4.4 Optical functions at the interaction points

Table 4 gives the statistics for the β-functions in the interaction points (the values for the ideal machine being $\beta_x^* = 1.5\,\text{m}$, $\beta_y^* = 0.05\,\text{m}$).   Each machine in the ensemble has had its vertical β-function corrected by a procedure that mimics the one followed in operation. The values for the imperfect machine are "measured" after orbit correction. A matching calculation is carried out using the ideal machine model to find increments of the QS0 quadrupoles that would produce these values.   The negatives of these increments are then applied to the quadrupoles.

Quantity		Mean	σ(est)	Units
Horizontal β−function for e$^+$[IP2]	β_{x1}(IP2)$^+$	2.13	0.469	m
Horizontal β−function for e$^-$[IP2]	β_{x1}(IP2)$^-$	2.008	0.461	m
Horizontal β−function for e$^+$[IP4]	β_{x1}(IP4)$^+$	2.059	0.546	m
Horizontal β−function for e$^-$[IP4]	β_{x1}(IP4)$^-$	2.108	0.462	m
Horizontal β−function for e$^+$[IP6]	β_{x1}(IP6)$^+$	2.007	0.381	m
Horizontal β−function for e$^-$[IP6]	β_{x1}(IP6)$^-$	2.067	0.395	m
Horizontal β−function for e$^+$[IP8]	β_{x1}(IP8)$^+$	2.126	0.458	m
Horizontal β−function for e$^-$[IP8]	β_{x1}(IP8)$^-$	2.125	0.487	m
Vertical β−function for e$^+$[IP2]	β_{y2}(IP2)$^+$	0.05132	0.00164	m
Vertical β−function for e$^-$[IP2]	β_{y2}(IP2)$^-$	0.05051	0.00163	m
Vertical β−function for e$^+$[IP4]	β_{y2}(IP4)$^+$	0.04966	0.0019	m
Vertical β−function for e$^-$[IP4]	β_{y2}(IP4)$^-$	0.05773	0.00345	m
Vertical β−function for e$^+$[IP6]	β_{y2}(IP6)$^+$	0.04838	0.00117	m
Vertical β−function for e$^-$[IP6]	β_{y2}(IP6)$^-$	0.05825	0.0027	m
Vertical β−function for e$^+$[IP8]	β_{y2}(IP8)$^+$	0.05005	0.00154	m
Vertical β−function for e$^-$[IP8]	β_{y2}(IP8)$^-$	0.05505	0.00164	m

Table 4

5 Parameters of the beams

As a further consequence of the different orbits and optics among machines and between beams in a given machine, beam parameters determined by integrals along the 6-dimensional closed orbit can differ. This section summarises the statistical information for some of the most important beam parameters.

5.1 Energy loss and radiation damping

Table 5 is a summary of the values of selected parameters related to the energy lost by synchrotron radiation and the radiation damping. The energy lost per turn is slightly higher than given by the standard calculation [6] using synchrotron radiation integrals for a particle with constant nominal energy on the central trajectory passing through the centres of the elements. An additional few MeV of energy is lost as the closed orbit passes off-centre through quadrupoles and other elements because of energy sawtoothing and the imperfections.

The damping partition numbers are close to their nominal values, except in the vertical mode. The correlation plot between damping partition numbers for the two beams is shown in Figure 2.

Quantity	Symbol	Mean	σ(est)	Units
Beam energy for e^+	E_b^+	94.	0.	GeV
Beam energy for e^-	E_b^-	94.	0.	GeV
Average momentum deviation for e^+	δ_s^+	0.	0.	
Average momentum deviation for e^-	δ_s^-	0.	0.	
Energy loss per turn for e^+	U_0^+	2286.	0.488	MeV
Energy loss per turn for e^-	U_0^-	2286.	0.486	MeV
Horizontal damping partition for e^+	J_1^+	0.9995	0.0391	
Horizontal damping partition for e^-	J_1^-	1.012	0.0329	
Vertical damping partition for e^+	J_2^+	0.9906	0.0669	
Vertical damping partition for e^-	J_2^-	0.9927	0.0435	
Longitudinal damping partition for e^+	J_3^+	2.01	0.0847	
Longitudinal damping partition for e^-	J_3^-	1.995	0.0535	
Horizontal damping time for e^+	τ_1^+	0.007328	0.000284	sec
Hor. damping time in turns for e^+	τ_1^+/T_0^+	82.41	3.19	
Vertical damping time for e^+	τ_2^+	0.007419	0.000572	sec
Vert. damping time in turns for e^+	τ_2^+/T_0^+	83.43	6.43	
Longitudinal damping time for e^+	τ_3^+	0.003645	0.000152	sec
Long. damping time in turns for e^+	τ_3^+/T_0^+	40.99	1.71	

Table 5
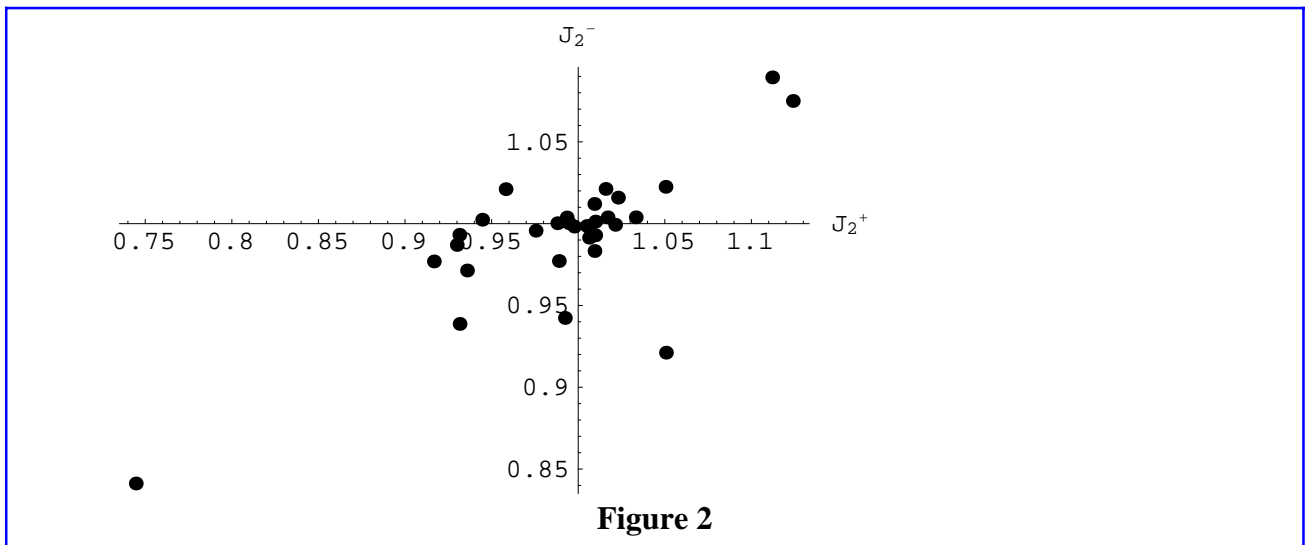
Figure 2

- Graphics -

It can be seen from the Figure 3 that, there is a non-linear correlation between the shift in the damping partition number and the RMS vertical dispersion around the ring. The change can be produced in strong quadrupoles where there is a combination of vertical orbit *and* dispersion.
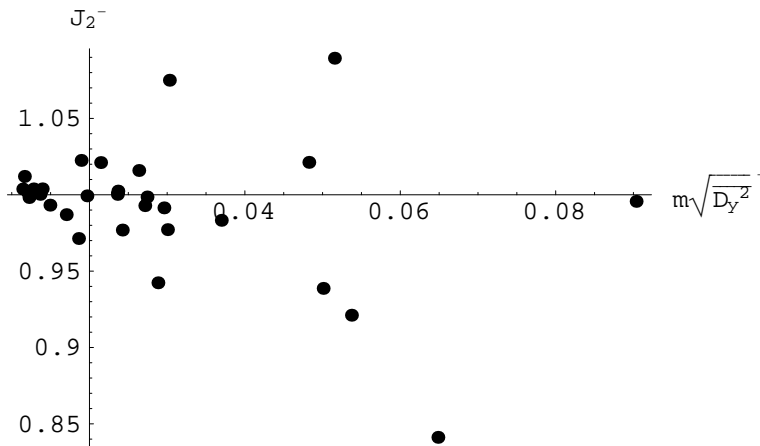
Figure 3

- Graphics -

5.2 Emittances and energy spread

Table 3 summarises the distributions of the emittances and related quantities.   The horizontal emittance has a rather small spread about its nominal value.

Quantity	Symbol	Mean	σ(est)	Units
Horizontal emittance for e^+	$\varepsilon_1{}^+$	28.84	1.96	nm
Horizontal emittance for e^-	$\varepsilon_1{}^-$	28.08	1.44	nm
Vertical emittance for e^+	$\varepsilon_2{}^+$	0.5132	0.49	nm
Vertical emittance for e^-	$\varepsilon_2{}^-$	0.4606	0.461	nm
Fractional energy spread for e^+	$\sigma_\epsilon{}^+$	0.001474	0.0000307	
Fractional energy spread for e^-	$\sigma_\epsilon{}^-$	0.001479	0.0000195	
Bunch length for e^+[IP2]	σ_z(IP2)$^+$	0.007012	0.000146	m

Table 6

If luminosity measurements are used to estimate the vertical emittance, then it is more reasonable to compare the *harmonic means*.   Indeed it is arguable that these are of greater physical relevance. (Recall that the harmonic mean of quantity *x* is $\langle x \rangle_{-1} = \langle x^{-1} \rangle^{-1}$ where $\langle x \rangle$ denotes the usual mean) a The harmonic means of the positron and electron emittances are

$$\langle \varepsilon_2{}^+ \rangle_{-1} = 0.234926 \, \text{nm}, \qquad \langle \varepsilon_2{}^- \rangle_{-1} = 0.173947 \, \text{nm}$$

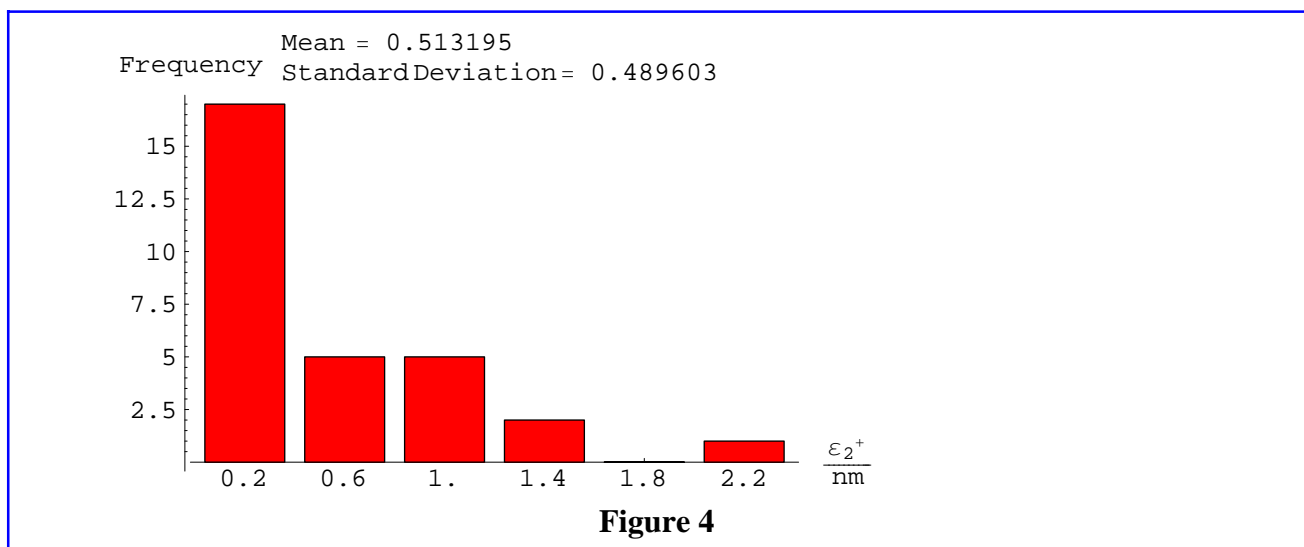The emittance ε_2 of the mainly-vertical mode is critical for the performance of the machine. The present simulation includes most optical effects that generate it (except the electrostatic separation bumps) but it should be kept in mind that the emittances given in Table 3 are the result of a *linear* eigenvector calculation.   Roughly speaking, the linear vertical emittance has two components:

- The vertical emittance generated by linear coupling. This includes the transverse betatron coupling generated by solenoids and skew-quadrupole fields and the linear synchro-betatron coupling generated by dispersion at RF cavities.

- The intrinsic vertical emittance generated by quantum excitation in locations where there is a magnetic field and a non-zero value of the optical function β_{y3} (or "dispersion"). The contribution of this effect to the emittance is inversely proportional to the vertical damping rate.

It has been shown [2] that the true vertical emittance may be larger than given by the linear calculation because of nonlinear effects. Quantum tracking results are not reported here.

Compared with other optics treated in a similar way, the emittances of the positrons and electrons are not always well-matched (see Figure 5, in which the solid line is the diagonal $x = y$, not a fit). This could lead to the emittances being over-estimated from luminosity measurements as compared to direct measurements on a given beam.
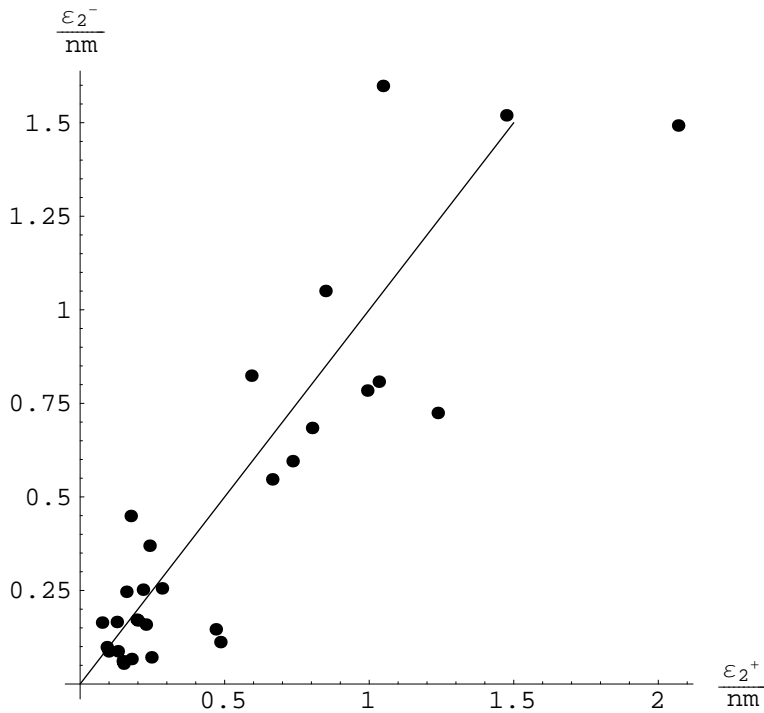
Figure 4

- Graphics -

Figure 5

- Graphics -

Since $\varepsilon_2 \propto \langle D_y^2 \rangle / J_2$, one would expect that some part of the distribution of vertical emittances can be attributed to the variation of the damping partition number of the mainly-vertical mode between machines (see Figure 2). However both the vertical quantum excitation and the damping partition depend on the vertical dispersion function. A plot of the vertical emittance against the RMS vertical dispersion, Figure 6, suggests a power-law behaviour

$$\varepsilon_2 \propto \left(\overline{D_y^2}\right)^{p/2}. \tag{1}$$
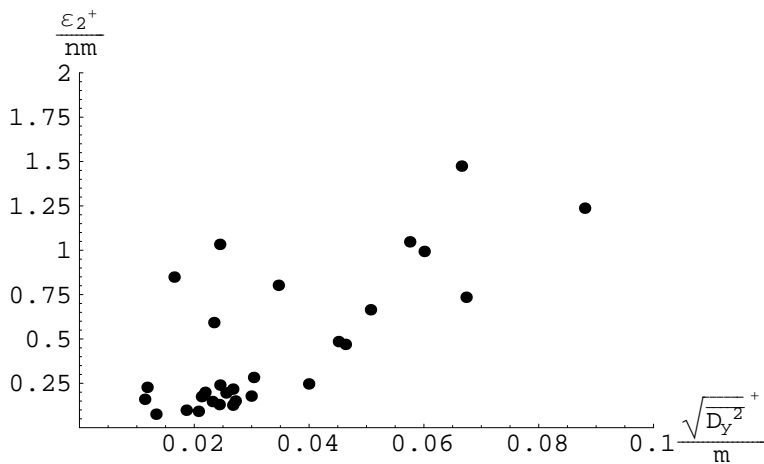
Figure 6

- Graphics -

To extract the power p, which we expect to be somewhat larger than 2, we can plot the Pearson correlation, r_P, between the left and right-hand sides of (1) as a function of p. The two curves in the following figure are obtained from the positron and electron data.

Figure 7
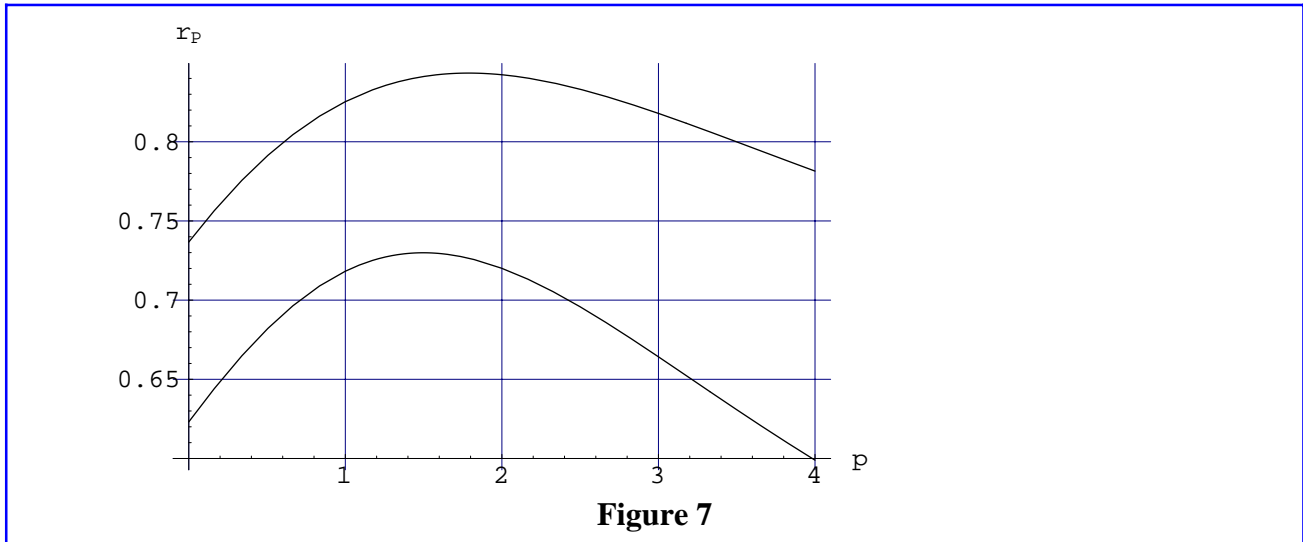
- Graphics -

The maxima of the two curves occur at

$$\{1.78725, 1.49778\}$$

$$p = 1.79 \qquad \text{and} \qquad p = 1.50 \tag{2}$$

and, taking the average of these two values, we can postulate an empirical formula for the vertical emittance in terms of the RMS vertical dispersion. A fit including a constant term to take account of residual betatron coupling gives

$$\frac{\varepsilon_2}{\text{nm}} == 77.5936 \left(\frac{D_y^{\text{rms}}}{m} \right)^{1.65} + 0.130398$$

and this is plotted, together with the data for both beams ("*" for e^+) in Figure 8. This formula is to be interpreted in a statistical sense. It may well be that the vertical emittance is particularly sensitive to the values of the vertical dispersion function in certain locations.
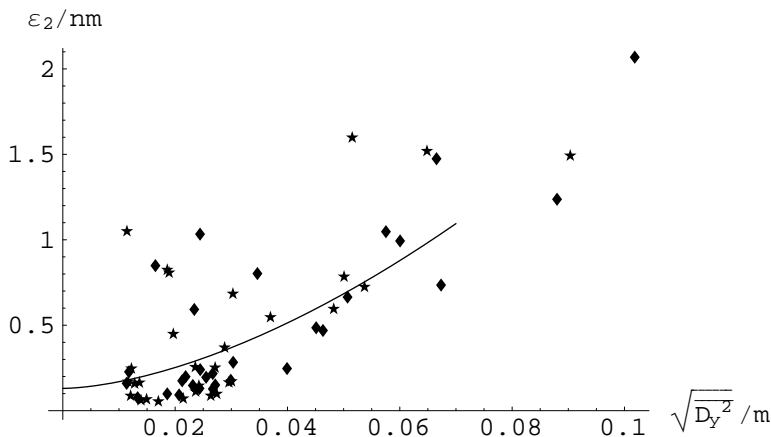
ε_2/nm

$\sqrt{\overline{D_y^2}}\,/\text{m}$

Figure 8

- Graphics -

The numerical coefficient in the fit is appropriate for an RMS vertical dispersion measured all around the ring - the numerical coefficient will be different for an average restricted to the pickups.

6 Dynamic Aperture

The transverse dynamic apertures A_x, A_y are defined as the largest stable initial values of the "Courant-Snyder invariants". These are just twice the action variables of the first two eigenmodes of linear oscillation (roughly speaking, the "horizontal and vertical betatron motion") about the 6-dimensional closed orbit and are expressed in units of metres. The emittances are the averages of the actions over the beam distribution. The projection of the dynamic aperture of the third mode ("synchrotron motion") is entirely analogous but is customarily converted to a dimensionless form in which it's square root can be interpreted as the amplitude of a fractional momentum deviation in percent.

In LEP, it is convenient and has become customary to quote the *square roots* of the dynamic aperture projections rather than the quantities themselves.

The following summary table shows that this optics has a large dynamic aperture in the mainly-horizontal mode:

| Quantity		Mean	σ(est)
Horizontal dynamic aperture	$10^3\sqrt{A_x/m}$	0.8283	0.144
Vertical dynamic aperture	$10^3\sqrt{A_y/m}$	1.277	0.201
Longitudinal dynamic aperture	$\sqrt{A_t}/\%$	0.961	0.211

Figure 9 provides a graphical impression of the distribution of the 4D dynamic aperture surfaces projected into the space of of amplitudes of the three normal modes. To avoid cluttering the figure too much, only the first 6 of the 27 dynamic apertures are shown. However they are quite representative of the full ensemble. The outermost surface is the dynamic aperture of the perfect machine. The ellipsoidal surface representing the beam has projections on the axes corresponding to $(10\,\sigma_1, 10\,\sigma_2, 7\,\sigma_3)$ derived from the linear emittances. It is shown purely to indicate the scale of the

dynamic aperture and plays no role in the calculation. The surface shown actually corresponds to the beam parameters of the third machine in the ensemble which happens to have $\varepsilon_2{}^+ = 0.49$ nm. In this case the beam ellipse extends far outside the dynamic aperture for the horizontal and longitudinal modes, indicating that the beam lifetime would be very short.
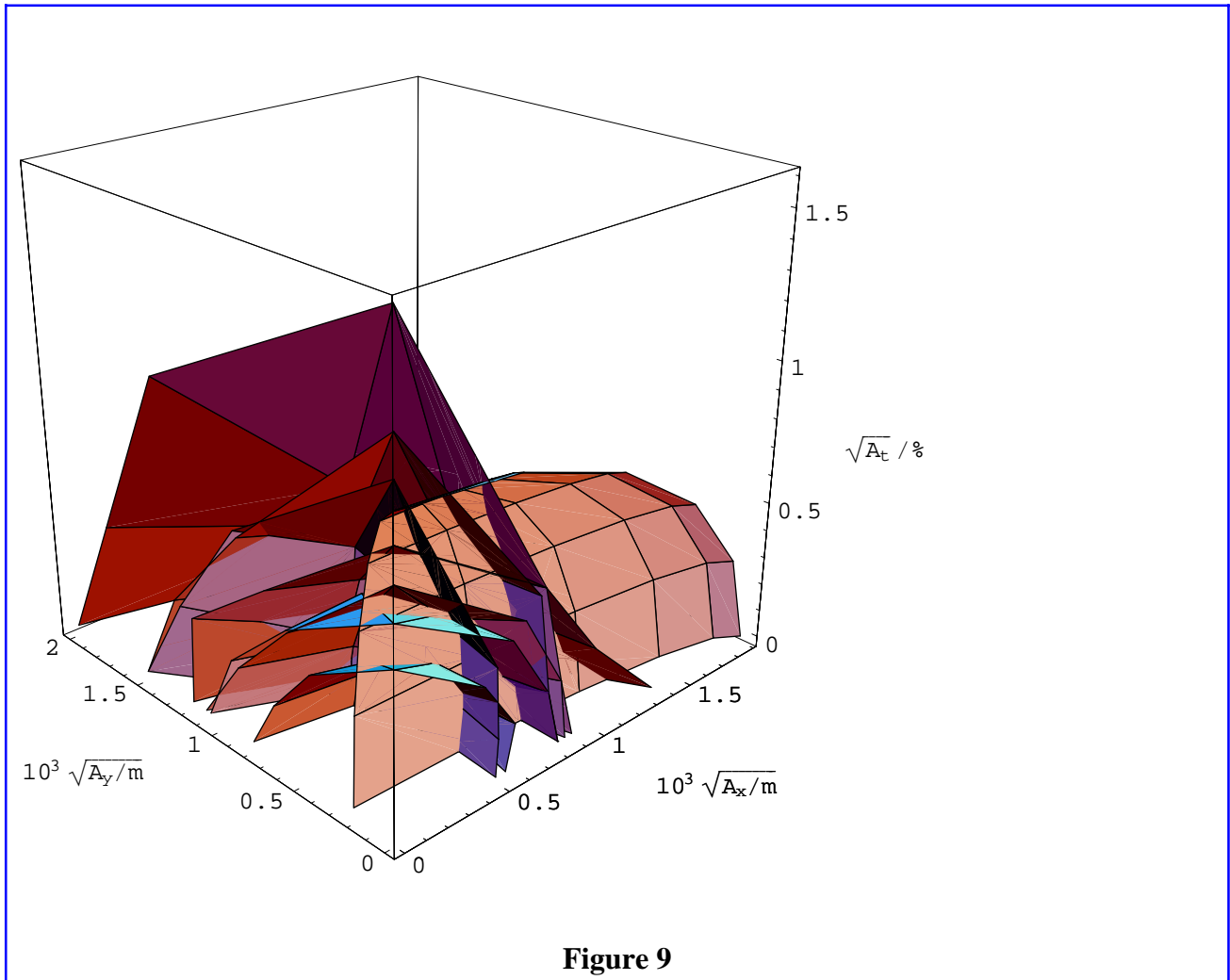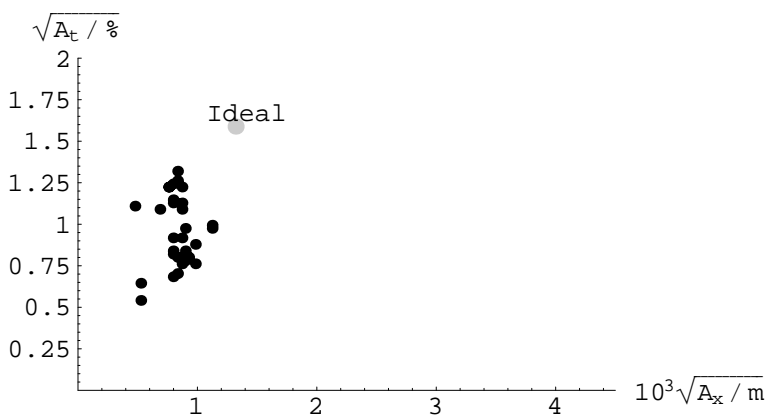

Figure 9

- Graphics3D **-**

We can also plot the correlations of the intersections of these surfaces with pairs of axes. For comparison, a point representing the ideal machine is included.
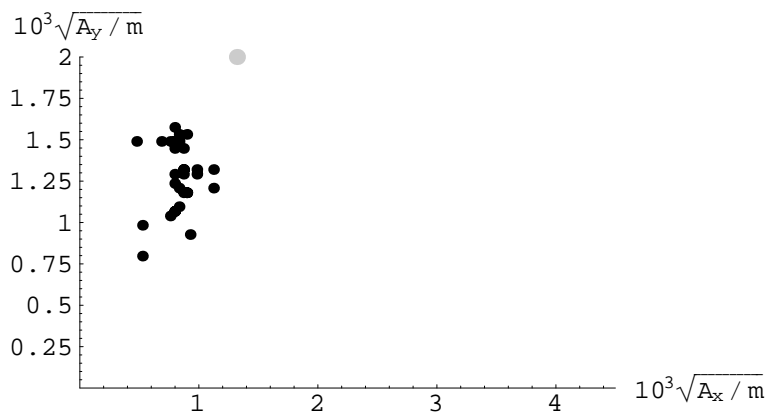
Figure 10

- Graphics -

There is no particular correlation between the horizontal dynamic aperture and the momentum acceptance (Figure 11). Indeed further exploration of the database of imperfect machines reveals no particular correlations of dynamic aperture components with quantities such as the emittances, dispersions, tunes or chromaticities.

Figure 11

7 Conclusions

The proposed LEP optics with $\mu_x = 131°$ and $\mu_y = 90°$ in the arc cells will almost certainly not work at 94 GeV or higheer energies. The dynamic aperture (in both horizontal betatron and synchrotron phases planes) is too small, varying betwen 2.5 and 6.1 σ_x in the ensemble of 30 corrected imperfect machines. Even in the case of a perfect machine it was found to be only $7.2\sigma_x$. The situation is even worse in the longitudinal plane so increasing the horizontal damping partition number is not an option. I have not conducted detailed studies of the instability mechanisms but they are almost certainly related to the strong *negative* detuning with amplitude and various imperfection-driven resonances. From past experience one can plausibly infer that there will be strong non-Gaussian beam tails that will further exacerbate the lifetime problems.

The calculations have been repeated for another version of the optics where the SF sextupoles were adjusted to reduce the detuning with amplitude. The results are very similar and will not be given in detail here (they are available to anyone interested).

Making the crude assumption that the horizontal dynamic is about the same at all energies, the maximum energy for which beams could be stored in this optics would be about 30 GeV. These predictions are consistent with the experimental results reported in [7].

7.1 Acknowledgements

My thanks to André Verdier for providing the optics files and for stimulating discussions.

8 References

[1] J.M. Jowett, *Monte-Carlo Study of the (102°,90°) Physics Optics for LEP*, CERN SL Note 97-84 (AP), and http://wwwslap.cern.ch/~jowett/lep97/mu10290by5A/SLNote97-84.html

[2] J.M. Jowett, *Vertical Beamsize (and other calculations) in Various Optics*, in Proc. 8th LEP Performance, Chamonix, January 1998, CERN-SL-98-006 (1998) http://www.cern.ch/CERN/Divisions/SL/publications/chamx98/PAPERS/JJ3_032.PDF

[3] Hans Grote, F. Christoph Iselin, The MAD Program, User'sReference Manual, CERN/SL/90-13 (AP), and http://wwwslap.cern.ch/~fci/mad/mad.html

[4] http://wwwslap.cern.ch/~jowett/JMJdocs.html

[5] J.M. Jowett, *Dynamic Aperture for LEP: physics and calculations*, in J. Poole (Ed.), Proc. 4th LEP Performance Workshop, CERN SL/94-06 (DI).

[6] M. Sands, *The Physics of Electron Storage Rings*, SLAC-121 (1970).

[7] M. Lamont, G. Roy, A. Verdier, Commissioning of the 131/90 lattice, SL-Note-98-059 MD (1998).